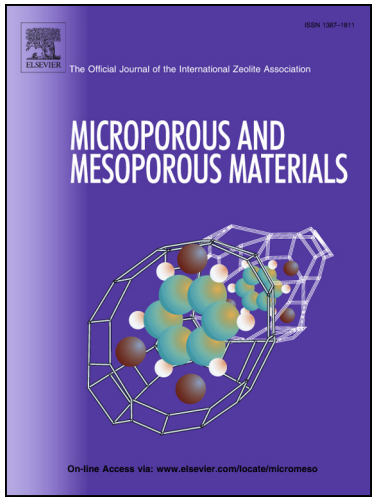

Gas phase imidazole methylation on zeolites and HPA/SiO_2: Study of acid site requirements and catalyst deactivation

M.N. Vanoy-Villamil, C.R. Apesteguía, C.L. Padró

PII: S1387-1811(13)00352-1
DOI: http://dx.doi.org/10.1016/j.micromeso.2013.07.016
Reference: MICMAT 6139

To appear in: *Microporous and Mesoporous Materials*

Received Date: 28 May 2013
Revised Date: 8 July 2013
Accepted Date: 9 July 2013

Please cite this article as: M.N. Vanoy-Villamil, C.R. Apesteguía, C.L. Padró, Gas phase imidazole methylation on zeolites and HPA/SiO_2: Study of acid site requirements and catalyst deactivation, *Microporous and Mesoporous Materials* (2013), doi: http://dx.doi.org/10.1016/j.micromeso.2013.07.016

Gas phase imidazole methylation on zeolites and HPA/SiO_2: Study of acid site requirements and catalyst deactivation

M.N. Vanoy-Villamil, C.R. Apesteguía, C.L. Padró*

Catalysis Science and Engineering Research Group (GICIC)

Instituto de Investigaciones en Catálisis y Petroquímica -INCAPE-(UNL-CONICET)

Santiago del Estero 2654, (3000) Santa Fe, Argentina.

*** Corresponding author**

Prof. Cristina Padró
INCAPE, Santiago del Estero 2654
(3000) Santa Fe, Argentina
Email: cpadro@fiq.unl.edu.ar
Website: www.fiq.unl.edu.ar/gicic

Abstract

The gas-phase alkylation of imidazole with methanol was studied at 523 K on solid acids such as HPA/SiO_2 and zeolites HMCM22, HBEA, NaY, ZnY and HY. The nature, density and strength of acid sites were determined by temperature programmed desorption of NH_3 coupled with infrared spectra of adsorbed pyridine. Coke formation was studied by temperature programmed oxidation technique. On all the samples, the selectivity to N-methylimidazole was greater than 98%. Catalysts presenting essentially Lewis (NaY and ZnY) or Brønsted (HPA/SiO_2) acidity did not promote efficiently the methylation of imidazole and yielded less than 20% of N-methylimidazole. In contrast, on samples containing similar concentration of Lewis and Brønsted acid sites (HY, HBEA, HMCM22) the N-methylimidazole yield was between 60 % (HMCM22) and 100% (HY). All the samples deactivated during the 4 h catalytic tests and formed significant amounts of coke, between 2.3% (NaY) and 8% (ZnY). Catalytic tests performed at different contact times showed that the initial activity decay diminished with increasing imidazole conversion, suggesting that catalyst deactivation is mainly related with the presence of the reactants, methanol and/or imidazole. In order to gain insight on the catalyst deactivation mechanism, additional catalytic tests using different feed compositions were performed. They showed that the initial catalyst deactivation followed a linear correlation with the partial pressure of imidazole which indicated that the activity decay is essentially related with strong adsorption of imidazole the on surface acid sites.

Keywords: Imidazole methylation, N-methylimidazole, catalyst deactivation, solid acids, deactivation mechanism.

1. Introduction

The N-alkylation of heterocyclic compounds, such as imidazole or pirazole, lead to the formation of valuable products widely used in pharmaceutical, agrochemical, food and cosmetic industries [1,2,3]. In particular, the alkylation of 1-3 azoles, like imidazole, is involved in the synthesis of anticonvulsants, bactericides, fungicides and protozoacidals compounds [4, 5, 6]. N-Methylimidazole, the main product of imidazole methylation, has diverse applications. For example, it is a raw material in the synthesis of N-methylimidazole polyamides [7], ionic liquids [8], and polymers for chromatographic columns [9]. It is also used as catalyst in acetylation reactions [10] and cocatalyst for the synthesis of cyclic carbonates from carbon dioxide and epoxides [11]. Furthermore, N-methylimidazole is a modifier of the acylation and alkylation activities of enzymes like Candida antarctica (CAL-B) [12] and Penicillin G acylase (PGA) [13] (the addition of 10% N-methylimidazole causes an over 70-fold increase in PGA activity).

Alkylimidazoles are commonly obtained by liquid-phase alkylation of imidazole using alkyl halides or dialkyl sulfates as alkylating agents and liquid bases such as NaOH or $NaNH_2$ as catalysts. These alkylating agents are highly toxic and cause corrosion; in addition, when combined with liquid bases form metal salts as by-products [14]. Thus, the development of novel ecofriendly processes using solid catalysts is a highly desirable technological target for the synthesis of alkylimidazoles. In liquid phase, the alkylation of imidazole with alkyl halides has been studied on solid

bases and acid zeolites, and N-alkylimidazole yields of up to 80% have been reported [15,16]. In gas phase, there is little information about the alkylation of imidazole with alcohols. In particular, only few papers have dealt with the imidazole alkylation with methanol on solid catalysts. For example, it has been reported that Mg-Al mixed oxides catalyze selectively the methylation of imidazol producing 90% of N-methylimidazole at 613 K, although the N-methylimidazole selectivity strongly decreases at lower temperatures [17]. Ono et al. [18] reported that acid zeolites, such as zeolites HY, HZSM5, HBEA and HMOR may produce 100% N-methylimidazole at 553 K. However, it is well known that acid zeolites often suffer from strong deactivation on stream when used in similar alkylation reactions [19, 20]. In spite of that, no studies have been reported yet dealing specifically with the deactivation of acid zeolites employed for the imidazole alkylation reaction.

In this paper we studied the vapor-phase alkylation of imidazole with methanol on solid acids to produce N-methylimidazole (Eq. 1). The reaction was carried out on

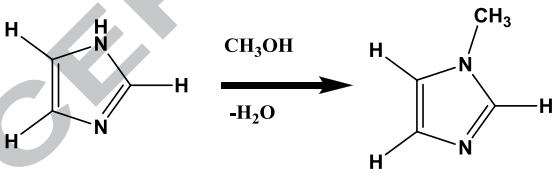

Eq. 1

HPA/SiO_2 and zeolites HMCM22, HBEA, NaY, ZnY and HY at different operating conditions. Our objectives were twofold: i) to ascertain the nature of the surface acid sites required for obtaining high N-methylimidazole yields; (ii) to gain insight on the catalyst deactivation mechanism by identifying the species responsible for the catalyst activity decay.

2. Experimental

2.1. Catalyst Preparation

Commercial samples of zeolites NaY (UOP-Y 54, Si/Al=2.4) and HBEA (Zeocat PB/H) were used. Zeolite HY was prepared by double ion exchange of zeolite NaY with a 1M NH_4Cl (Merck, 99.8%) aqueous solution at 333 K. Zeolite ZnY was obtained by triple ion exchange of zeolite NaY with 0.5 M $Zn(NO_3).6H_2O$ (Riedel-de Haën, 98%) solution at 353 K. Zeolite HMCM22 was synthesized according to [21] by using sodium aluminate (Alfa Aesar, Technical Grade), silica (Aerosil Degussa 380), sodium hydroxide (Merck, >99%), hexamethyleneimine (Aldrich, 99%) and deionized water as reagents. The gel molar composition was SiO_2/Al_2O_3=30, OH/SiO_2=0.18, hexamethyleneimine/SiO_2=0.35 and H_2O/SiO_2=45. The crystallization of the gel was conducted in a teflon lined stainless steel autoclave at 423 K during 7 days with stirring. HPA/SiO_2 was obtained by wet impregnation. A suspension of SiO_2 powder (Grace G62, 99.7%; 230 m^2g^{-1}) was stirred in an aqueous solution of HPA ($H_3PW_{12}O_{40}.6H_2O$, Merck P.A) at room temperature for 24 h. Before reaction, all the samples were treated in air (60 cm^3min^{-1}) at 723 K during 3 h, except HPA/SiO_2 that was treated at 573 K for 2 h.

2.2. Catalysts characterization

BET surface areas were measured by physisorption of N_2 at 77 K in a Autosorb Quantochrome Instrument 1-C sorptometer. The chemical composition of the samples were determined by Atomic Absorption Spectroscopy.

Density, strength and nature of surface acid sites were studied by temperature-programmed desorption (TPD) of NH_3 and FTIR of adsorbed pyridine. Previous to the ammonia adsorption, the samples (100 mg) were treated in helium at 773 K for 2 h. HPA/SiO_2 was pretreated at 573 K for 2 h.

The adsorption of NH_3 was carried out at 373 K using a 1%NH_3-99%He mixture. The physisorbed NH_3 was eliminated by flushing with He at 373 K during 90 min. Finally, the temperature was increased at 10 $K.min^{-1}$ in a He flow of 60 $cm^3.min^{-1}$ and desorbed ammonia was analyzed by mass spectrometry (MS) in a Baltzers Omnistar unit.

Infrared measurements were performed on a Shimadzu FTIR Prestige-21 spectrophotometer. The catalysts were ground to a fine powder and pressed into wafers (10-30 mg). The discs were mounted in a quartz sample holder and transferred to an inverted T-shaped Pyrex cell equipped with CaF_2 windows. The samples were outgassed in vacuum at 723 K during 2 h and cooled to 298 K under evacuation. Due to the low thermal stability of HPA/SiO_2 (acid structure of HPA decomposes at 723 K) this sample was heated in vacuum at 573 K before pyridine adsorption. Spectra were recorded at room temperature, after admission of pyridine, adsorption at room temperature and sequential evacuation at 423 K and 573 K (423 K and 473 K for HPA/SiO_2).

Coke formed on the catalysts during reaction was studied by temperature programmed oxidation (TPO). Samples (20-100 mg) were heated from room

temperature to 1073 K at 10 K.min^{-1} in a 3%O_2-97%N_2 stream. The CO_2 formed by coke combustion was converted into methane passing through a methanation catalyst (Ni/kieselghur) at 673 K. The methane was analyzed using a flame ionization detector (gas chromatograph: SRI 8610C).

2.3. Catalytic activity

The gas phase alkylation of imidazole (Aldrich, >99%) with methanol (Merck, 99.8%) was carried out in a fixed bed continuous flow reactor at 523 K and 101.3 kPa. Samples (0.35-0.42 mm) were treated in situ at 723 K in air flow for 2 h before reaction. Imidazole (IMI) and methanol (M) were fed as a solution (M/IMI=10) using a syringe pump (Cole-Parmer EW-74900) and vaporized in a preheated N_2 stream to give a N_2 / (IMI+M) ratio of 30 and a contact time W/F^0_{IMI} = 451.1 g.h.mol^{-1}. The exit gas composition was analyzed on-line every 20 min during 4 h using an Agilent 6850 chromatograph equipped with a flame ionization detector and a 30 m Innowax column (inner diameter: 0.32 mm, film thickness: 0.5 μm). Imidazole conversion (X_{IMI}) and selectivity to product *i* from imidazole (S_i) were calculated as: $X_{IMI} = \Sigma Y_i / (\Sigma Y_i + Y_{IMI})$ and S_i (mol of product *i*/mol of imidazole reacted) = $[Y_i/\Sigma Y_i]$, where Y_i is the molar fraction of products formed from imidazole, and Y_{IMI} is the outlet molar fraction of imidazole. Yields (η_i, mol of product *i*/mol of imidazole fed) were obtained as $\eta_i = S_i \cdot X_{IMI}$. Methanol conversion ($X_M$) and selectivity to dimehtylether (S_{DME}, mol of methanol converted to DME/ mol of methanol converted) were determined as:

$X_M = (Y_M^0 - Y_M)/Y_M^0$ and $S_{DME} = Y_{DME} * 2/(Y_M^0 - Y_M)$ where Y_M^0 and Y_M are the molar fraction of methanol at the entrance of the reactor and the molar fraction at the exit, respectively and Y_{DME} is the outlet molar fraction of dimethylether. Considering the IMI/M ratio used in the experiences, the maximum methanol conversion to alkylation products (correspondig to a X_{IMI} =100%) would be 10%.

Additional experiences in order to determine the influence of the feed composition on catalyst deactivation were carried out at 523 K and 101.3 kPa by varying molar ratio of imidazole-methanol solution. In these experiments the contact time was varied between 40 and 70 g.h.mol^{-1} in order to keep the conversion of imidazole under 15%.

3. Results and Discussion

3.1. Catalyst characterization

The chemical composition and surface area of the catalysts are shown in Table 1. The exchange of zeolite NaY with H^+ and Zn^{2+} cations diminished the sodium content from 7.5 % to 0.3% (HY) and 0.4 % (ZnY), which corresponds to exchange degrees of 96 and 95%, respectively. The exchange treatments decreased the surface area of parent NaY zeolite (700 $m^2.g^{-1}$) to 660 $m^2.g^{-1}$ (HY) and 612 $m^2.g^{-1}$ (ZnY). In the case of sample HPA/SiO_2, the addition of 28 % wt of HPA caused a diminution in the surface area of SiO_2 from 230 $m^2.g^{-1}$ to 205 $m^2.g^{-1}$.

The sample acidity was studied by NH_3 TPD and FTIR using pyridine as a probe molecule. The NH_3 TPD profiles for all the samples used in this work are shown in Figure 1. The TPD curve of NaY displayed a single asymmetric peak with a maximum at about 480 K arising from ammonia adsorbed on weak and medium acid sites while zeolite HY presented and additional broad desorption band at higher temperatures indicating the presence of stronger acid sites. The evolved NH_3 from zeolite ZnY gave rise to the low-temperature peak at 480 K with a shoulder at about 550 K, and a wide desorption band at higher temperatures denoting that the exchange of zeolite NaY with Zn^{2+} not only increased the density of medium and weak acid sites but also generated strong acid sites. The NH_3 TPD curve of HMCM22 presented two well defined peaks at about 500 K and 650 K respectively. Zeolite HBEA exhibited moderate aciditiy with a peak at 500 K and a wide zone corresponding to the desorption of ammonia from stronger acid sites. The NH_3 desorption of HPA/SiO_2 gave rise to a broad desorption band in the 450-1000 K range with two peaks at about 510 K and 840 K, reflecting the presence of surface acid species that bind NH_3 with different strength. This broad strength distribution is probably the result of the HPA spreading on the silica surface that generates highly interacting heteropolyacid/support species. The high-temperature peak at 840 K indicates the preferential generation of strong acid sites, due to the increasing amount of HPA without interaction since pure HPA desorbs NH_3 in a single peak at 900 K [22].

The acid sites densities ($\mu mol.g^{-1}$) were determined by deconvolution and integration of the NH_3 TPD profiles in Figure 1 and are included in Table 2. Zeolites ZnY and HY showed the highest concentrations of acid sites per gram (2121 and 1430

μmol.g^{-1}, respectively) whereas HPA/SiO_2 presented the lowest acid site density (160 (μmol.g^{-1}).

The chemical nature, strength and density of surface acid sites were investigated by analyzing the FTIR spectra obtained after adsorption of pyridine at 298 K and evacuation at 423 K and 573 K. Pyridine adsorbed on Brønsted acid sites shows absorption bands at 1540 cm^{-1}, 1480-1500 cm^{-1} and 1640 cm^{-1} [23,24]. Pyridine coordinatively bonded on Lewis acid sites produces characteristic bands at 1440-1460 cm^{-1}, 1480-1500 cm^{-1} and 1600 cm^{-1}. The 1600 cm^{-1} band shifts to higher frequencies with the increase in the strength of the acid sites [25]. FTIR spectra after pyridine adsorption at 298 K and evacuation at 423 K are displayed in Figure 2. Zeolite NaY presented essentially Lewis acidity (absorption bands at 1445 cm^{-1}, 1490 cm^{-1} and 1600 cm^{-1}). The exchange of Na^+ by Zn^{2+} caused the disappearance of the 1445 cm^{-1} and 1600 cm^{-1} bands (pyridine adsorbed on Na^+ cations) and the development of two bands at 1455 cm^{-1} and 1615 cm^{-1} corresponding to pyridine coordinatively bonded on Zn^{2+} cations [26, 27]. The frequency shift from 1600 cm^{-1} (NaY) to 1615 cm^{-1} (ZnY) reflects the generation of stronger Lewis acid sites on zeolite ZnY. Finally, the FTIR spectra of zeolites HY, HBEA and HMCM22 showed the contribution of both Lewis (bands at 1455 and 1620 cm^{-1}) and Brønsted acid sites (bands at 1540 and 1635 cm^{-1}).

The relative contibution of Lewis and Brønsted acid sites after evacuation of pyridine at 423 K and 573 K was obtained by integration of the bands at 1445-1455 cm^{-1} (Lewis) and 1540 cm^{-1}(Brønsted); results are presented in Table 2. Zeolites NaY and ZnY (L/B=32) presented essentially Lewis acidity. The Py-523K/Py-423K ratio (i.e. the ratio of the amounts of pyridine remaining on the sample after evacuation at 523 K and 423 K) were 0.73 and 0.35 on ZnY and NaY, respectively, revealing that ZnY contains

stronger Lewis acid sites than NaY. This result is consistent with the shape of the NH_3 TPD curves presented for these two zeolites in Figure 1. After outgassing at 423 K, L/B ratios of 1.5, 1.0 and 0.3 were determined for zeolites HY, HBEA and HMCM22, respectively. The Py-523K/Py-423K ratio was 0.77 on HMCM22 and about 0.5 for HY and HBEA, thereby indicating that HMCM22 presented stronger acid sites. HPA/SiO_2 contained mainly Brønsted acid sites; L/B ratios of 0.16 and 0.14 were in fact determined after sample evacuation at 423 K and 473 K, respectively. The presence of pyridine adsorbed on Lewis acid sites of HPA/SiO_2 suggests that upon impregnation of HPA on SiO_2, the heteropolyacid partially transforms giving rise to lacunary or unsaturated species of Lewis acid character formed by interaction with the silica support [28].

3.2. Catalytic results for methylation of imidazole

3.2.1 Catalyst activity

On all the catalysts, N-methylimidazole was the main product of the gas-phase alkylation of imidazole with methanol. The selectivity to this product was always higher than 98%. Products formed by dehydration and condensation of methanol, such as dimethylether and light hydrocarbons, were also observed.

In Figure 3, we plotted the N-methylimidazole yield ($\eta_{N\text{-}MI}$) as a function of time on stream for all the catalysts studied in this work. Results in Figure 3 show that the methylation of imidazole over solid acids strongly depends on the nature and strength of surface acid sites. On NaY, the initial N-methylimidazole yield (η^{o}_{NMI}), obtained by

extrapolating at t=0 the η_{NMI} vs *t* curve, was only 4.6% (Table 3). This result indicated that the weak Lewis acid sites present in zeolite NaY were not suitable to efficiently promote the N-alkylation reaction. Zeolite ZnY that contains almost exclusively Lewis acid sites although stronger than NaY, presented also low activity for producing N-methylimidazole. The η^0_{NMI} value on ZnY was in fact only 19.2%. Nevertheless, zeolites NaY and ZnY were active for converting methanol; as shown in Table 3, the initial methanol conversions were 45 % (NaY) and 59% (ZnY). On the other hand, HPA/SiO_2, which contains mainly strong Brønsted acid sites (L/B=0.16), showed also low activity for the alkylation reaction despite that methanol conversion reached 67%. The most active catalyst for imidazole methylation was zeolite HY that yielded 100% imidazole at the beginning of reaction. Zeolite HY has high density of strong acid sites with a L/B ratio of 1.5 (Table 2). The η^0_{NMI} values obtained on zeolites HBEA (L/B=1) and HMCM22 (L/B=0.32) were 74.1% and 59.8 %, respectively. In contrast, methanol conversion followed an opposite order: 49% and 71% for HBEA and HMCM22, respectively (Table 3). Overall, data in Figure 3 and Table 3 show that the methylation of imidazole is preferentially promoted on zeolites containing a similar concentration of Lewis and Brønsted acid sites. This result is in agreement with previous reports on the gas-phase phenol methylation over acid zeolites [29,30,31].

3.2.2 Catalyst deactivation

Results reported in Figure 3 and Table 3 showed that all the catalysts deactivated on stream. In Figure 4 we plotted the activity (a_{NMI}) as a function of time;

a_{NMI} is defined as $a_{NMI} = r_{NMI}/r^0_{NMI}$ where r^0_{NMI} and r_{NMI} are the rate of N-methylimidazole formation at t=0 and t=t, respectively. From the initial slopes of curves a_{NMI} vs *t* in Figure 4 we determined the parameter $d_0 = -[da_{NMI}/dt]_{t=0}$ that accounts for the initial catalyst deactivation [32]; the obtained d_0 values are included in Table 3. The highest d_0 values (about $15x10^{-3}$ min^{-1}) were determined for NaY and HPA/SiO_2 samples while the lowest initial deactivation was observed for zeolite HBEA (d_0 = 1.8 $x10^{-3}$ min^{-1}). Zeolites ZnY and HMCM22 presented similar d_0 values of about $11x10^{-3}$ min^{-1}.

The observed catalyst activity decay on stream could be caused by both coke formation from parallel/consecutive reactions of reactants/products, and strong adsorption of reactants/products on surface active sites In order to obtain insight on catalyst deactivation mechanism we characterized the carbonaceous deposits by performing temperature programmed oxidation experiments. Previous to TPO characterization, samples recovered from the catalytic runs showed in Figure 4, were treated at 523 K in N_2 during 30 minutes. The obtained TPO profiles are shown in Figure 5. The TPO curve for HMCM22 exhibited a low-temperature peak at 423 K and a broad combustion band between 573 K and 1073 K. The low-temperature peak probably arises from carbon deposits with high H/C ratio retained in the small channels of this zeolite. HBEA presented a small oxidation peak at 443 K and two peaks at 823 K and 953 K. The TPO profiles of HPA/SiO_2, HY and NaY showed similar oxidation bands between 723 and 923 K. ZnY showed a big broad band of combustion that begins at 700 K and ends at about 1030 K. The amounts of coke formed during reaction were calculated from the area under the TPO curves of Figure 5 and are included in

Table 3 as %C. Significant coke were formed on the catalysts, between 2.3 % (NaY) and 8 % (ZnY).

In an attempt to find a relationship between the deactivation kinetics and the amount of coke formed on the catalysts we plotted in Figure 6 the initial deactivation parameter d_0 as a function of % C and of mol of C/mol of acid site. From the data in Figure 6 is clear that there is not a linear correlation between the catalyst activity decay and the amount of coke.

To obtain more insight on the species responsible for catalyst deactivation, additional catalytic tests at different contact times, between 40 and 88 g h/mol, were carried out on zeolite HBEA. In Figure 7 we have represented the values of d_0 determined from these catalytic tests (not shown here) as a function of contact time. It is observed that d_0 diminished when the contact time was increased, thereby suggesting that catalyst deactivation is mainly related with the presence of the reactants, methanol and/or imidazole.

The formation of coke from methanol decomposition on solid acids has been studied by other authors [33, 34, 35, 36, 37]. Methanol is initially dehydrated to dimethylether on either Brønsted or Lewis acid sites and then ligth hydrocarbons such as methane, ethene, ethane, propane and propene, and aromatics may be formed, preferentially on Brønsted acid sites [38]. Here, we observed the formation of dimethylether on all the catalysts during the imidazole methylation reaction. Formation of light hydrocarbons was observed only on ZnY whereas heavier hydrocarbons were exclusively detected on catalysts containing strong Brønsted acidity (protonic zeolites and HPA/SiO_2).

Imidazole, the other reactant, is an amphoteric compound that can act either as an acid or a base. As an acid (pKa 14.5) is less acidic than carboxylic acids but more acidic than alcohols. The acidic proton is attached to N-1. As a base (pKa of conjugated acid, 7.1) is sixty times more basic than pyridine (pKa of conjugated acid, 5.25) and the basic site is the N-3, the nitrogen with a free electron pair. Protonation of imidazole gives the imidazolium cation which is highly symmetric. Based in its chemical properties, it is expected that imidazole will adsorb on surface acid sites either by coordinating their free electrons to Lewis acid sites or by protonation on Brønsted acid sites. These interactions may be strong enough to deactivate the catalyst acid sites.

3.2.3 Effect of the feed composition on catalyst deactivation

The effect of feed composition on catalyst deactivation was studied on HBEA at 523 K and 101.3 kPa. The contact time was varied between between 40 and 70 g.h.mol^{-1} in order to keep the conversion of imidazole below 15% in all the catalytic tests. We first determined the reaction orders for imidazole methylation by using a power-law rate equation:

$$r_{NMI}^{0} = k\, P_{IMI}^{\alpha}\, P_{M}^{\beta} \qquad \text{Eq. (2)}$$

where P_{IMI}^{α} and P_{M}^{β} are the partial pressure of imidazole and methanol in the feed, respectively. The observed catalyst deactivation on stream required that the initial conversion rate of imidazole (r_{NMI}^{0}) be determined by extrapolating the η_{NMI} vs time curves (not shown here) to initial time-on-stream. The α value was measured by varying

the imidazole partial pressure between 0.21 and 0.52 kPa at a fixed methanol pressure (2.5 kPa). Similarly, reaction order β was obtained by varying P_M between 1.71 and 3.05 kPa while keeping P_{IMI} at 0.25 kPa. The plots representing log r^0_{NMI} as a function of log P_{IMI} and log P_M are shown in Figure 8. Reaction orders α and β were determined graphically from the plots of Figure 8. The reaction order with respect to methanol was close to 0.8 while the reaction order in imidazole was negative (-0.23). These reaction order values are consistent with a reaction mechanism where both, methanol and imidazole, adsorb and compete for the surface acid sites being the imidazole adsorption stronger.

From the η_{NMI} vs t curves obtained here by varying the partial pressures of methanol and imidazole, we also determined the initial deactivation parameter, d_0, for all the catalytic tests. In Figure 9 we have plotted the obtained d_0 values as a function of P_{IMI} and P_M. It is observed that d_0 was directly proportional to P_{IMI} (Figure 9 A) while no clear relationship was found between d_0 and P_M (Figure 9 B). These results strongly suggest that the catalyst deactivation kinetics observed during imidazole methylation is essentially related with the strong adsorption of imidazole on the surface acid sites of the catalyst.

4. Conclusions

The catalyst activity for the gas-phase alkylation of imidazole with methanol strongly depends on the nature and strength of the surface acid sites. HPA/SiO_2 (strong Brønsted sites) and zeolites NaY (weak Lewis acidity) and ZnY (strong Lewis aciditiy) that contain essentially only one type of acid sites do not promote efficiently imidazole methylation. In contrast, zeolites containing a similar concentration of Lewis and Brønsted acid sites such as HY, HMCM22 and HBEA are highly active and selective for this reaction yielding up to 100% of N-methylimidazole at 523 K (zeolite HY).

All the catalysts form coke and undergo significant losses of activity on stream. However, the catalyst activity decay does not follow a linear correlation with the amount of coke formed on the catalyst. The initial catalyst deactivation diminishes when the contact time is increased, thereby indicating that the activity decay reflects mainly the loss of active sites by the strong adsorption of reactants. The reaction orders with respect to imidazole and methanol on zeolite HBEA were -0.23 and 0.8, respectively, which indicated a stronger adsorption of imidazole. Actually, the initial deactivation of HBEA for imidazole alkylation followed a linear relationship with imidazole partial pressure, thereby suggesting that the imidazole adsorption step plays a fundamental role in the catalyst deactivation mechanism.

Acknowledgments

This work was supported by the Universidad Nacional del Litoral (UNL), Consejo Nacional de Investigaciones Científicas y Técnicas (CONICET), and Agencia Nacional de Promoción Científica y Tecnológica (ANPCyT), Argentina.

References

[1] J. Weitkamp, M. Hunger, U. Rymsa, Micropor. Mesopor. Mater. 48 (2001) 255-270.

[2] H. Hattori, Appl. Catal. A. 222 (2001) 247-259.

[3] R.A. Sheldon, R. S. Downing, Appl. Catal. A 189 (2) (1999) 163-183.

[4] D.R. Hirschfield. Eur. Patent. Appl. EP 91 (1983) 289.

[5] S. Khabnadideh, Z. Rezaei, A. Khalafi-Nezhad, R. Bahrinajafi, R. Mohamadia, A.A. Farrokhroza, Bioorg. Med. Chem. Lett. 13 (2003) 2863.

[6] K. Walker, US Patent US 4.059.705 (1977).

[7] K. Shinohara, T. Bando, H. Sugiyama, Anticancer Drugs, 2010 21 (3) (2010) 228-242.

[8] J.S. Wilkes, Green Chem. 4 (2002) 73-80.

[9] Y. Li, Y. Chen, K. Wang, L. Nie, S. Yao, Electrophoresis 33 (13) (2012) 2005-2011.

[10] J. Wu, M. Li, J. Lin, D. Wei, J. Chromatogr. Sci. 49 (5) (2011) 375-378.

[11] D. Ji, X. Lu, R. He, Appl. Catal. A 203 (2000) 329-333

[12] B. Liu, A. Wu, J.Xu, X. Lin, Chem Commun (Camb).21;(3) (2007) :295-297.

[13] B. Liu, Q. Wu, D. Lv, X. Lin, J. Biotechnol. 20, 153 (3-4) (2011) 111-115.

[14]. Y. Ono, Y. Izawa, Z-H. Fu, Catal. Lett. 47 (1997) 251-253

[15] J.M. López-Pestaña, J. Díaz-Terán, M.J. Avila-Rey, M.L. Rojas-Cervantes, R.M. Martín-Aranda, Microp. Mesop. Mat. 67(2004) 87-94

[16] V. Calvino-Casilda, R.M. Martín-Aranda, A.J. López-Peinado, M. Bejblová and J. Čejka, Appl. Catal. 338 (2008) 130-135.

[17] H. Grabowska, M. Zawadzki, L. Syper , W. Mista, Appl. Catal. A: Gen. 292 (2005) 208

[18] Y. Ono, Z-H, Fu, Y. Izawa, in H.K. Beyer, H.G. Karge, I. Kiricsi and J.B. Nagy (Eds.) Catalysis by Microporous Materials, Stud. Surf. Sci. Catal. Vol. 94 (1995) 697-704

[19] J.L. Sotelo, M. A. Uguina, J. L. Valverde, D. P. Serrano, Appl. Catal. A: Gen. 114 (1994) 273-285

[20] A. Feller, J-O. Barth, A. Guzman, I. Zuazo, J.A. Lercher, J. Catal. 220 (2003) 192-206

[21] M.K. Rubin, P. Chu, US Patent 4,954,325, 1990

[22] V.K. Díez, B.J. Marcos, C.R. Apesteguía, J.I. Di Cosimo, Appl. Catal. A: Gen 358 (2009) 95-102.

[23] E.P. Parry, J. Catal. 2 (1963) 371-379.

[24] H. Knözinger, Adv. Catal. 25 (1976) 184-271.

[25] G. Busca, Catal. Today 41 (1998) 191-206.

[26] J. Penzien, A. Abraham, J. van Bokhoven, A. Jentys, T. Müller, C. Sievers, J.J. Lercher, J. Phys. Chem. B 108 (2004) 4116-4126.

[27] C.L. Padró, E.A. Rey, L.F. González Peña, C.R. Apesteguía 143 (2011) 236-242

[28] V.K. Díez, C.R. Apesteguía, J.I. Di Cosimo, Catal. Lett. 123 (2008) 213-219.

[29] E. Santacesaria, D. Grasso, d. Gelosa, S. Carrá, Appl. Catal. 64 (1990) 83-99

[30] L.F. González Peña, M.E. Sad, C.L. Padró, C.R. Apesteguía, Catal. Lett. 141 (2011) 939-947

[31] M. E. Sad, C.L.Padró, C.R. Apesteguía, Catal. Today 133-135 (2008) 720-728

[32] C.L. Padró, C.R. Apesteguía, Catal. Today 107–108 (2005) 258–265

[33] H. Knözinger, K. Kochloeft, W. Meyer, J. Catal. 28 (1973) 69

[34] H. Knözinger, D. Dautzenberg, J. Catal. 3 (1974) 142.

[35] T. Tsoncheva, R. Dimitrova, Appl. Catal. A. Gen 225 (2002) 101.

[36] S.H. Campbell, X-Z Jiang, R.F. Howe, Micropor. Mesopor. Mater. 29 (1999) 91.

[37] V. Vishwanathan, K-W Jun, J-W Kim, H-S Roh, Appl. Catal. A. Gen 276 (2004) 251.

[38] F.S. Ramos, A.M. Duarte de Farias, L.E.P. Borges, J.L.Monteiro, M.A. Fraga, E.F. Sousa-Aguiar, L.G. Appel, Catal. Today 101 (2005) 39-44

Figures Captions

Figure 1: TPD profiles of NH_3. Heating rate, 10 K/min

Figure 2: FTIR spectra of pyridine adsorbed at 298 K and evacuated at 423 K

Figure 3: N-Methylimidazole yield as a function of time on stream. HY (●), HBEA (△), HMCM22 (◆), ZnY (O), HPA/SiO_2 (◇) NaY(▲) [T= 523 K, W/F^0_{IMI} =451.16 g h mol^{-1} ; IMI/M=0.1, N_2/(IMI+M) = 30];

Figure 4: Activity decay for N-Methylimidazole formation (α) as a function of time on stream. HY (●), HBEA (△), HMCM22 (◆), ZnY (O), HPA/SiO_2 (◇) NaY(▲). [T= 523 K, W/F^0_{IMI} =451.16 g h mol^{-1} , IMI/M=0.1, N_2/(IMI+M) = 30]

Figure 5: TPO profiles . Heating rate: 10 K. min^{-1}

Figure 6: Catalyst initial deactivation (d_0) versus % C (empty symbols) and mol of carbon per mol of acid sites (full symbols). Samples recovered from the catalytic runs showed in Figure 4 : HY(●,○) HBEA (◆,◇), HMCM22 (▼,▽), ZnY(▲,△), HPA/SiO_2(■,□) and NaY (◀,◁).

Figure 7: Catalyst initial deactivation (d_0) as a function of contact time [Catalyst: HBEA; T=523 K ; IMI/M=0.1, N_2/(IMI+M) = 30]

Figure 8: Dependence of imidazole conversion rate upon imidazole (A) and methanol (B) partial pressures. [T=523 K, P = 101.3 kPa]

Figure 9: Dependence of catalyst initial deactivation upon imidazole (A) and methanol (B) partial pressures [T=523 K, P = 101.3 kPa]

Figure 1

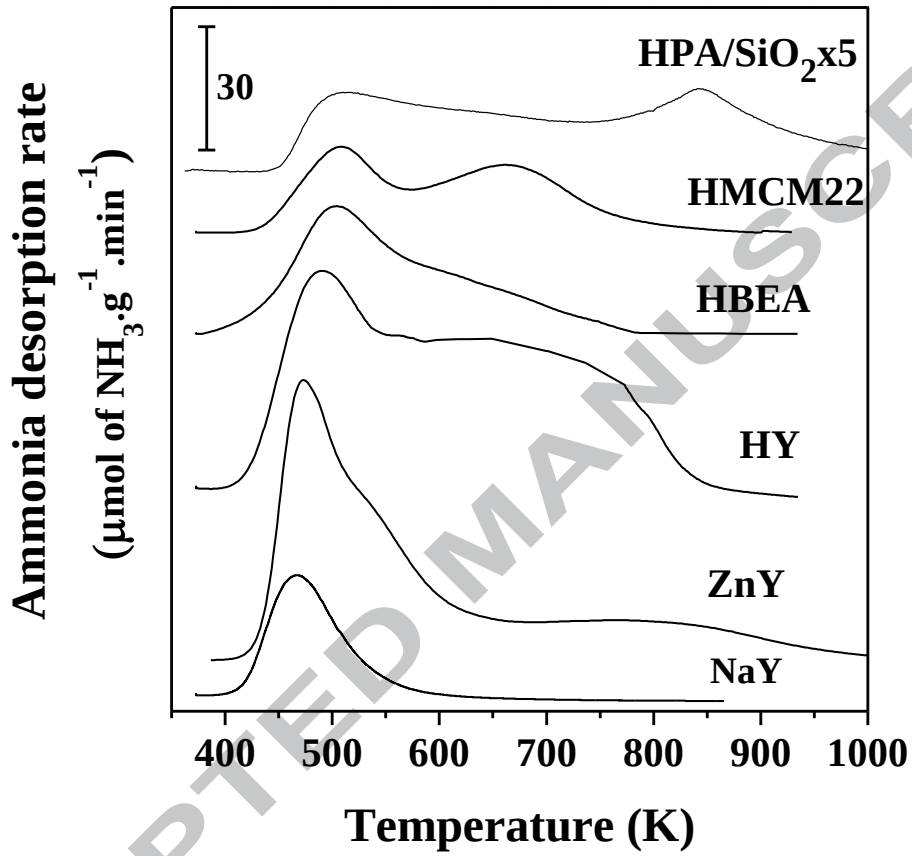

Figure 2

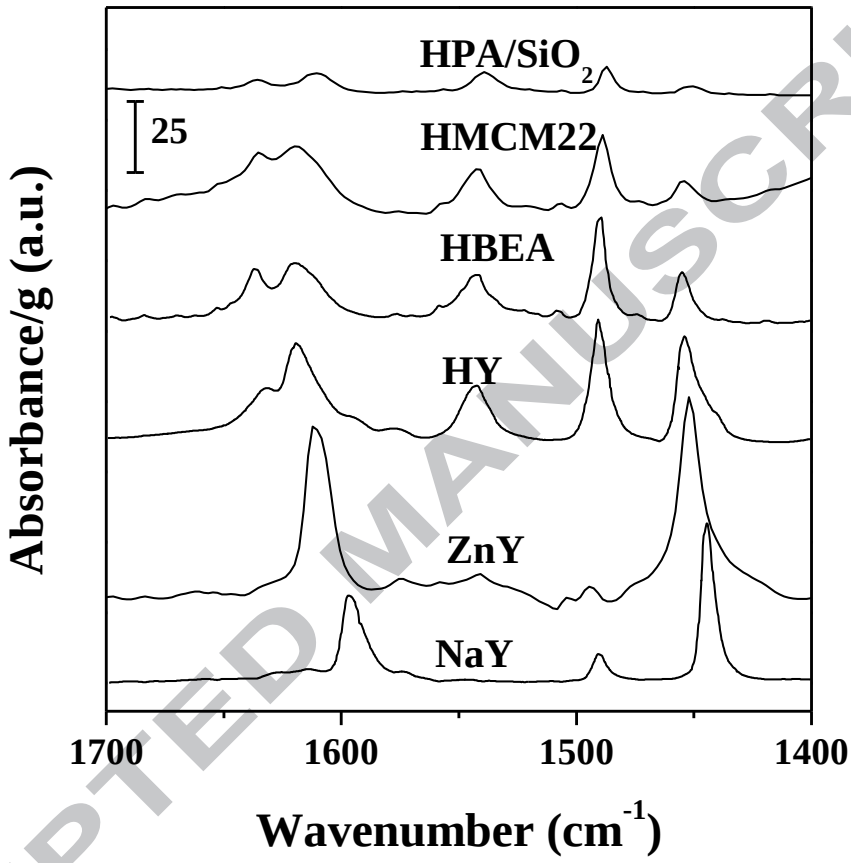

Figure 3

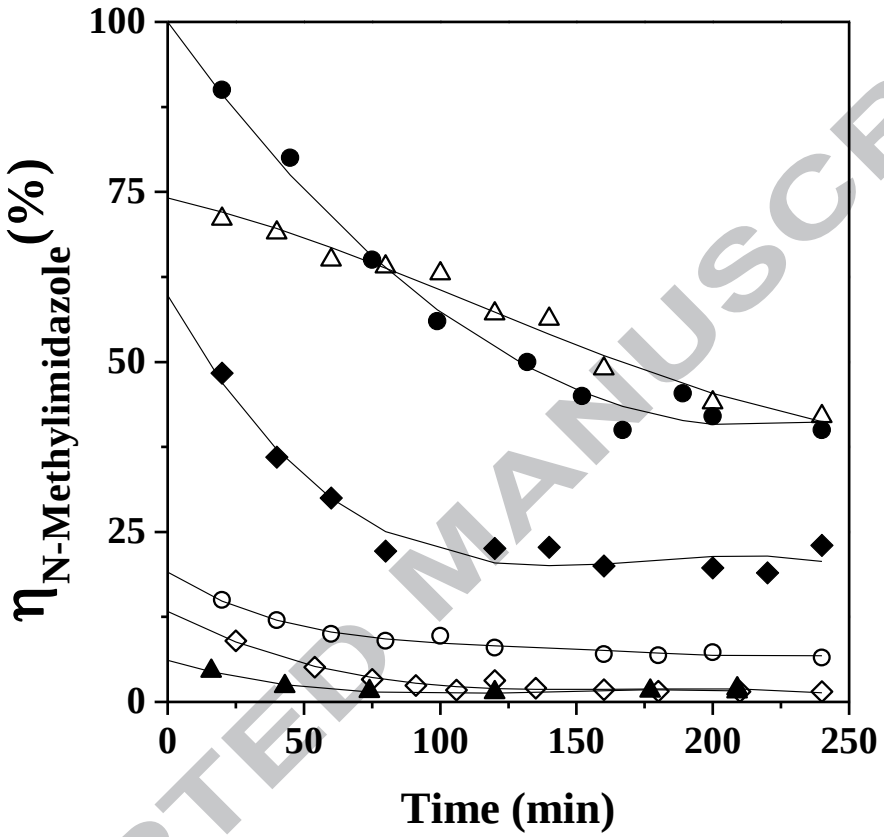

Figure 4

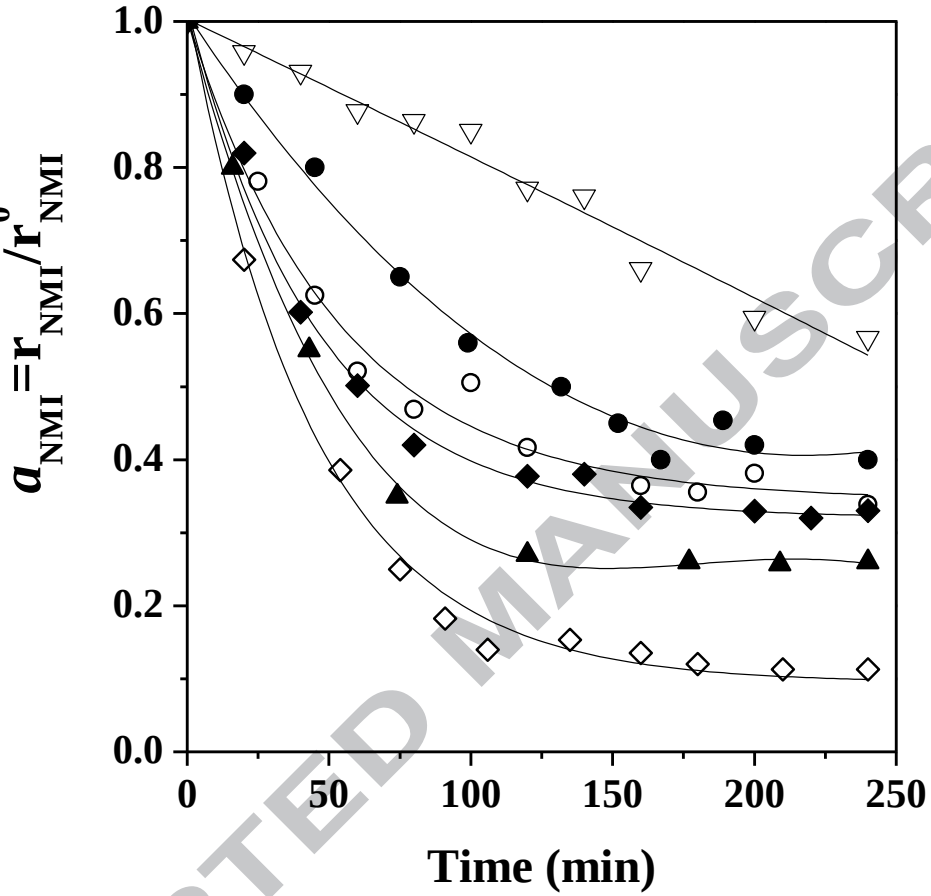

Figure 5

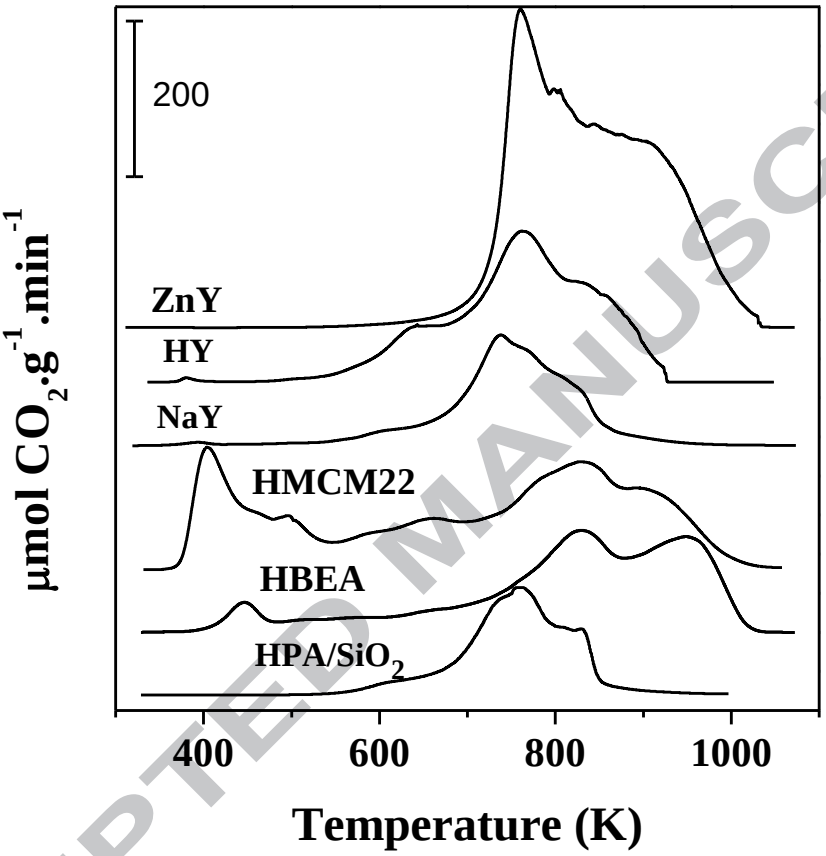

Figure 6

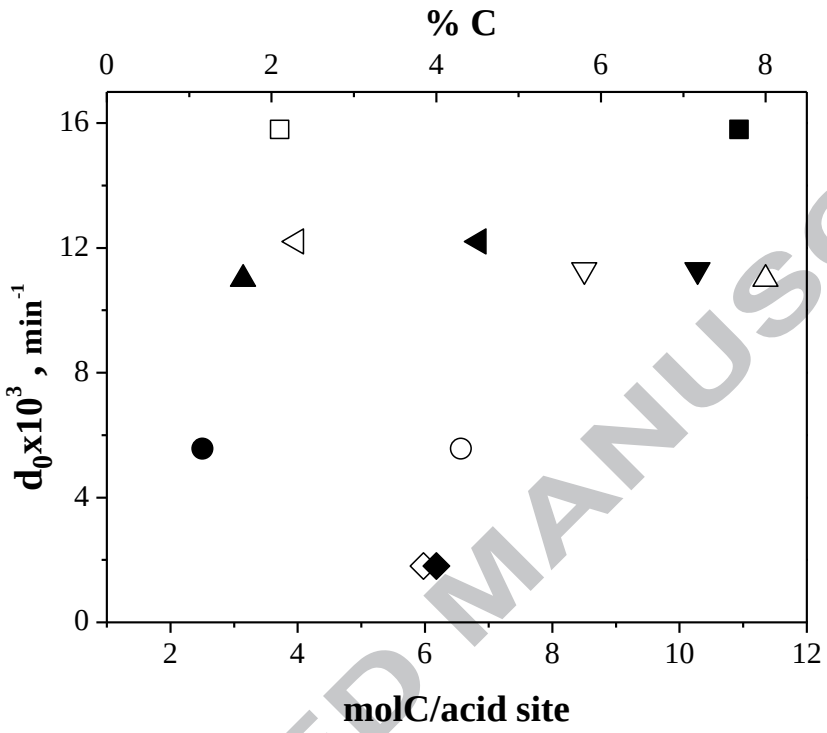

Figure 7

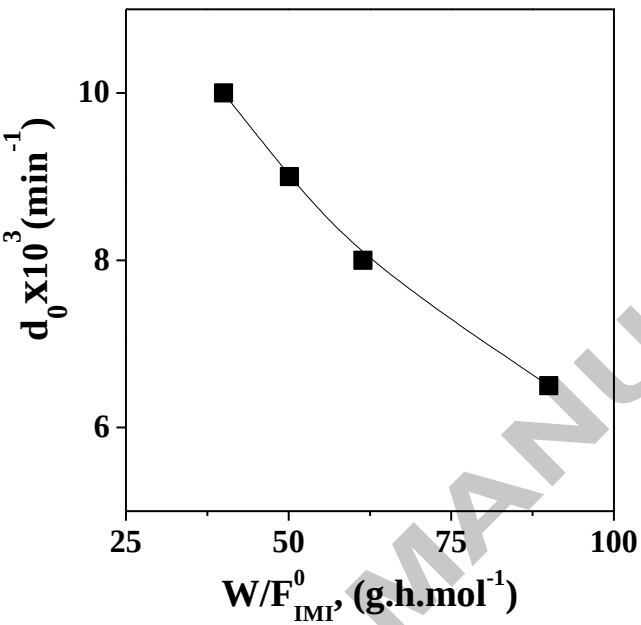

Figure 8

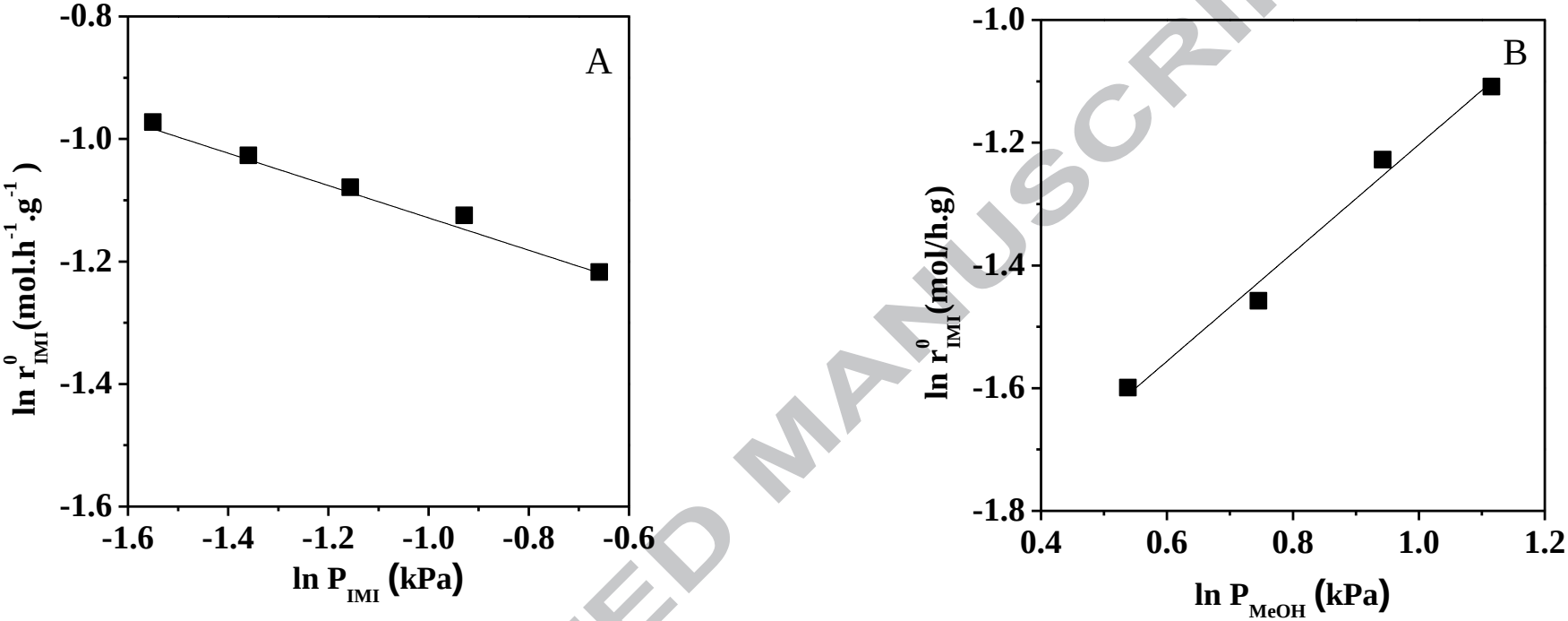

Figure 9

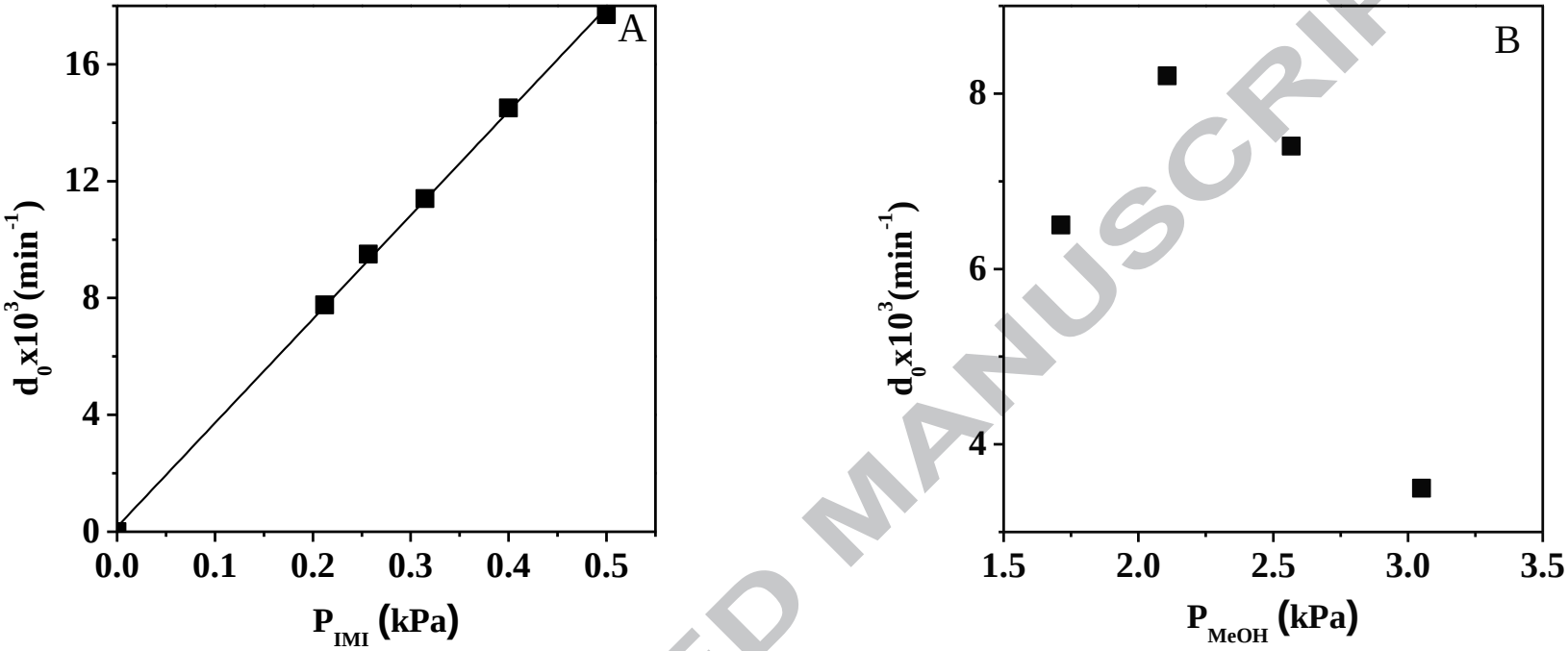

Table 1: Chemical composition and surface area of the samples used in this work

Samples	Chemical composition				S_{BET}
	Na (wt %)	Zn (wt %)	HPA (wt %)	Si/Al (molar ratio)	($m^2.g^{-1}$)
HBEA	0.04	-	-	12.5	560
NaY	7.5	-	-	2.4	700
HY	0.3	-	-	2.4	660
ZnY	0.4	9.3	-	2.4	612
HMCM22	-	-	-	15.0	400
HPA/SiO_2	-	-	28	-	205

Table 2: Sample Acidity

Sample	TPD of NH_3	FTIR of pyridine				
	Acid site density ($\mu mol.g^{-1}$)	$T_{desorption}$=423 K			$T_{desorption}$=573 K	
		Brønsted sites (B) ($area.g^{-1}$)	Lewis sites (L) ($area.g^{-1}$)	L/B	Brønsted sites ($area.g^{-1}$)	Lewis sites ($area.g^{-1}$)
HBEA	558	150	151	1	74	92
NaY	280	-	525	-	-	181
HY	1430	310	465	1.5	209	177
ZnY	2121	37	1200	32	9	880
HMCM22	470	560	176	0.32	444	120
HPA/SiO_2	160	91	15	0.16	70 [a]	10 [a]

[a] $T_{desorption}$= 473 K

Table 3: Catalytic results for the gas-phase alkylation of imidazole with methanol

Catalyst	N-methylimidazole yield, %		Methanol conversion, %		Dimethyleter selectivity, %	Catalyst deactivation	
	t = 0h	t = 4h	t = 0h	t = 4h	t = 0h	$d_0 x 10^3$ (min^{-1})	%C
HBEA	74.1	42.0	49	36	54	1.8	4.0
NaY	4.6	0.8	45	43	48	12.2	2.3
HY	100.0	40.1	70	38	60	5.6	4.3
ZnY	19.2	6.5	59	47	22	11.0	8.0
HMCM22	59.8	19.7	71	38	55	11.3	5.8
HPA/SiO_2	13.3	1.5	67	35	41	15.8	2.1

T= 523 K, W/F^0_{IMI} =451.16 g.h.mol^{-1}, IMI/M=0.1, N_2/(IMI+M) = 30

d_0 (initial deactivation)=$[d\alpha/dt]_{t=0}$

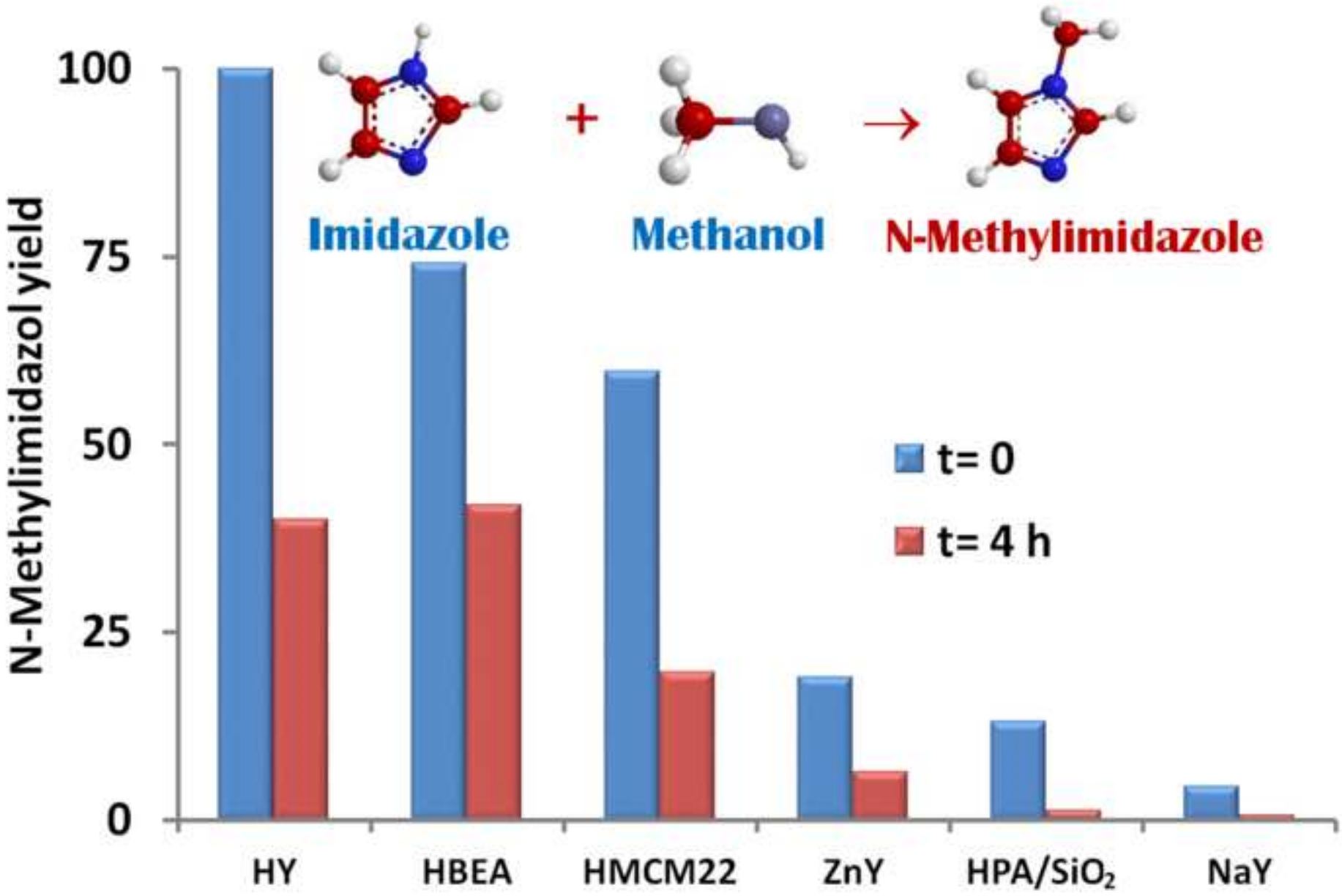

Zeolites containing Lewis and Brønsted acid sites promote imidazole methylation
All the catalysts deactivate during catalytic tests and form coke.
Activity decay follow a linear correlation with the partial pressure of imidazole
Deactivation is related with the strong adsorption of imidazole on acid sites.